Distributed Cooperative Control for Multi-UAV Flying Formation

Belkacem Kada, Abdullah Y.Tameem, Ahmed A. Alzubairi, Uzair Ansari
Aerospace Engineering Department, King Abdulaziz University Jeddah, KSA

***Abstract*—The problem of collaborative pattern tracking in multi-agent systems (MAS) like unmanned aerial vehicles (UAV) is investigated in this article. First, a new method for distributed consensus is constructed inside the framework of the leader-following approach for second-order nonlinear MAS. The technique canceled the chattering effect observed in the conventional sliding mode-based control protocols by transmitting smooth input signals to agents' control channels. Second, a novel formation framework is proposed to accomplish three-dimensional formation tracking by including consensus procedures in the formation dynamics model. This will allow for formation tracking in all three dimensions. The Lyapunov theory provides evidence demonstrating the proposed protocols' stability and convergence. Numerical simulations have been carried out to prove the proposed algorithms' effectiveness.**

Keywords*—Formation control; distributed consensus; multi-agent systems; multiple-UAV

I. Introduction

The increased complexity of the missions of engineering systems has led to the development of distributed and cooperative control for networked systems under the paradigm of multi-agent systems (MAS). The benefits of using MAS include increased efficiency, precision, flexibility, robustness, and affordability. Real-life applications of MAS include ground systems [1], [2]. , unmanned aerial vehicles (UAV) [3]–[12], transport aircraft [13], [14], helicopters [15], spacecraft [16]–[19], satellites [20], [21], and missiles [22], [23].

One of the most fascinating and challenging applications of networked aerial systems is the cooperative control of multi-UAV systems. Research on multi-UAV cooperative control has recently increased, employing various methods and theories. Using the net contract protocol, Liu & Zhang [3] developed a model for assigning tasks to manned and unmanned aerial vehicles in real environments. The formation control problem of multi-UAV systems was treated as a differential game problem in [4], with the open-loop Nash strategy for each agent being to construct fully distributed formation control. The creation of autonomous quadrotor aircraft was addressed in [5] by developing a non-smooth distributed cohesive motion control using the virtual structure approach. The non-smooth backstepping design technique was used to create a distributed formation flying control algorithms [6]. Using a differential evolution method, Zhang et al. [7] designed an adaptive formation control to find the optimum formation for a swarm of UAVs. An algorithm based on the Riccati equation was used in [8] to solve the problem of formation-containment control for a fleet of multirotor UAVs. Ziyang et al. [9] proposed a decentralized, self-organized mission planning algorithm. According to [10], a distributed formation control free of collisions can be created using a Voronoi diagram or partition. Path planning for a formation control approach with constraints and without collisions was examined in [11] utilizing rapid particle swarm optimization, considering chaos-based initialization, parameter optimization, and topology updating. For linear MAS, Almalki & Kada [24] offered a sliding-PID control that can be applied directly for multi-UAV consensus tracking.

Although the methodologies and approaches discussed above have been shown to be effective, there are still several critical obstacles to be solved in the cooperative control of MAS, particularly in multi-UAV systems. Formation keeping, communication failures inside MAS, altering communication topologies, and the smoothness of control inputs are some practical issues that must be addressed. Within the framework of a smoothly distributed consensus and formation control paradigm, we address these challenges and provide potential solutions in the study that we have presented here. As a result, the first thing we have contributed is the invention of distributed consensus procedures that are smooth for multi-agent systems with nonlinear dynamics integrated into them. In place of the signum-based control used in classic MAS control, which results in controller chattering, a continuous PI-like (proportional-integral) control is used to design the control inputs to the agent closed-loop dynamics. This allows for more precise and accurate control over the system. The second significant contribution made by this study is a model for maintaining airborne formation. We create the formation model by combining distributed protocols into a six-degree-of-freedom dynamical framework. This allows us to simulate the formation of complex structures. For a fair comparison, one can see, for example, the work presented in [25] and [26].

II. Preliminaries

Graph theory can be used to model the topology of information exchange in a networked system with n agents.

The interaction among an agent set $\mathcal{M} = \{1,2,\dots,n\}$ is represented by a weighted graph $\boldsymbol{\mathcal{G}} = (\mathcal{V}, \mathcal{E}, \mathcal{A})$ where $\mathcal{V} = (\mathcal{v}_1, \mathcal{v}_2, \dots, \mathcal{v}_n)$ denotes the vertex set, $\mathcal{E} \subseteq \mathcal{V} \times \mathcal{V}$ denotes an edge set, and $\mathcal{A} = \left(a_{ij} \geq 0\right) \in \mathbb{R}^{n\times n}$ describe a nonnegative adjacency matrix. The elements a_{ij} are defined such that $a_{ij} > 0$ if $\left(\mathcal{v}_i, \mathcal{v}_j\right) \in \mathcal{E}$, $a_{ij} = 0$ if $\left(\mathcal{v}_i, \mathcal{v}_j\right) \notin \mathcal{E}$, and $a_{ij} = 0$ (no self-loop).

Definition 1: Each agent i in the set $\mathcal{M}$ has a set of neighbors denoted by its connectivity set, $\mathcal{N}_i = \{\mathcal{v}_i | (\mathcal{v}_j, \mathcal{v}_i) \in \mathcal{E}\}$.

Definition 2 Laplacian matrix $\boldsymbol{L}(l_{ij}) \in \mathbb{R}^{n\times n}$ is associated with the graph $\mathcal{G}$, where $l_{ij} = -a_{ij}$ for $i \neq j$ and $l_{ij} = \sum_{j=1,j\neq i}^{n} a_{ij}$

Assumption 1: As the graph $\boldsymbol{\mathcal{G}}$ is not fully connected, the topology is directed communication that allows only the leader to communicate with the followers.

Unlike undirected communication, where a symmetric matrix comes from the exchange of information in both directions, directed communication involves a one-way flow of data (due to the symmetry of the coupling weights).

Assumption 2: When defining the Laplacian matrix , the eigenvalues $\lambda_i(\boldsymbol{\mathcal{L}})$ are specified as $0 \leq \lambda_1(\boldsymbol{\mathcal{L}}) < \lambda_2(\boldsymbol{\mathcal{L}}) < \cdots < \lambda_n(\boldsymbol{\mathcal{L}})$.

III. System Model

A. Distributed Consensus Problem for Nonlinear Second-Order MAS

MAS can be considered a team consisting of a single virtual leader 0 and a diverse set n of identically-behaving, second-order dynamics followers.

$$\begin{cases} \dot{\boldsymbol{x}}_i = \boldsymbol{\mathcal{v}}_i \\ \dot{\boldsymbol{\mathcal{v}}}_i = \boldsymbol{f}_i(t, \boldsymbol{x}_i, \boldsymbol{\mathcal{v}}_i) + \boldsymbol{u}_i \end{cases} \quad (1)$$

where the agent's position, velocity, and control input vectors are represent respectively by $\boldsymbol{x}_i, \boldsymbol{\mathcal{v}}_i, \boldsymbol{u}_i \in \mathbb{R}^m$, It is detailed how the dynamics of the virtual leader work by

$$\begin{cases} \dot{\boldsymbol{x}}_0 = \boldsymbol{\mathcal{v}}_0 \\ \dot{\boldsymbol{\mathcal{v}}}_0 = \boldsymbol{f}_0(t, \boldsymbol{x}_0) \end{cases} \quad (2)$$

where $\boldsymbol{x}_0, \boldsymbol{\mathcal{v}}_0 \in \mathbb{R}^m$ are the position and velocity of the leader. The dynamics of the leader and the followers are modeled by the functions $\boldsymbol{f}_0, \boldsymbol{f}_i \in \mathbb{R}^m$, respectively.

Assumption 3: System (1) is stabilizable if and only if the functions $\boldsymbol{f}_i$ are uniformly bounded with respect to t and locally uniformly bounded with respect to $\boldsymbol{x}_i$ and $\boldsymbol{\mathcal{v}}_i$. As a consequence of that,

$$\|\boldsymbol{f}_i(t, \boldsymbol{x}_i, \boldsymbol{\mathcal{v}}_i)\|_2 \leq \delta_{\boldsymbol{f}_i} \quad (3)$$

Where $\delta_{\boldsymbol{f}_i} \in \mathbb{R}^+$

B. Distributed Consensus Control Algorithm

Here, we examine the issue of smooth distributed consensus control for a second-order nonlinear MAS under the assumption of time-varying velocities. The aim of controlling is to design distributed individual protocols $\boldsymbol{u}_i$ that will lead to the following sort of consensus agreement:

$$\begin{cases} \lim_{t\to\infty} \|\boldsymbol{x}_i(t) - \boldsymbol{x}_0(t)\|_2 = 0 \\ \lim_{t\to\infty} \|\boldsymbol{\mathcal{v}}_i(t) - \boldsymbol{\mathcal{v}}_0(t)\|_2 = 0 \end{cases} \forall i \in \mathcal{v} \quad (4)$$

In order to find a solution to this consensus problem, we have come up with certain smooth distributed control protocols, which are as follows:

$$\boldsymbol{u}_i = -\alpha\, \boldsymbol{e}_i - \beta\, |\boldsymbol{e}_i|^{\gamma} \quad (5)$$

$$\boldsymbol{e}_i = \sum_{j=0}^{n} a_{ij}(\boldsymbol{x}_i - \boldsymbol{x}_j) + c \sum_{j=0}^{n} a_{ij}(\boldsymbol{\mathcal{v}}_i - \boldsymbol{\mathcal{v}}_j) \quad (6)$$

while α and β represent control gains and $c \in \mathbb{R}^+$ is constant, and the exponent γ is a positive constant chosen by the designer.

Assumption 4 There exists a constant $\delta_{\boldsymbol{L}} \in \mathbb{R}^+$ for which

$$\|\boldsymbol{L} \otimes \boldsymbol{I}_p\|_{\infty} \leq \delta_{\boldsymbol{L}} \lambda_{max}(\boldsymbol{L}) \quad (7)$$

Where $\boldsymbol{I}_p$ denotes the p-identity matrix, $p = n \times m$

Theorem 1 Let's suppose that assumptions 1–4 are valid, and that the communication graph $\boldsymbol{\mathcal{G}}$ is connected. It is possible that the parameters of the distributed protocols (5)-(7) can be satisfied if:

$$\begin{cases} \alpha < \frac{\beta \delta_{f_i}}{(1+c)\lambda_{max}(\boldsymbol{L} \otimes \boldsymbol{I}_p)} \\ \beta > \binom{\gamma}{0}^{-1} \frac{1}{\lambda_2^{\gamma+1}(\boldsymbol{L})} \left(\frac{2V_x(0)}{\lambda_{max}(\boldsymbol{L})}\right)^{1-\gamma} \\ \delta > 0 \end{cases} \quad (8)$$

Therefore, the consensus argument (4) is reached by a nonlinear leader-follower MAS (1)-(2). A Lyapunov function associated with the positions of the agents is indicated by $V_x(0) = V_x(t = 0)$, where λ is an eigenvalue.

Proof: The time dependence is left out of the notation for simplicity. Each piece of evidence is described in detail below.

First, let's define the vectors $\tilde{\boldsymbol{x}}_i = \boldsymbol{x}_i - \boldsymbol{x}_0 \in \mathbb{R}^m$, $\tilde{\boldsymbol{\mathcal{v}}}_i = \boldsymbol{\mathcal{v}}_i - \boldsymbol{\mathcal{v}}_0 \in \mathbb{R}^m$, $\tilde{\boldsymbol{\xi}}_x = [\tilde{\boldsymbol{x}}_1^T, \dots, \tilde{\boldsymbol{x}}_n^T]^T \in \mathbb{R}^p$, $\tilde{\boldsymbol{\xi}}_v = [\tilde{\boldsymbol{v}}_1^T, \dots, \tilde{\boldsymbol{v}}_n^T]^T \in \mathbb{R}^p$, $u = [\boldsymbol{u}_1^T, \dots, \boldsymbol{u}_n^T]^T \in \mathbb{R}^p$,where $p = n \times m$, the system of (3-1)–(3-2) is modified by applying those notation to be

$$\begin{cases} \dot{\tilde{\boldsymbol{\xi}}}_x = \tilde{\boldsymbol{\xi}}_v \\ \dot{\tilde{\boldsymbol{\xi}}}_v = \boldsymbol{f}(\tilde{\boldsymbol{\xi}}_v) + \boldsymbol{u} \end{cases} \quad (9)$$

Second, employing (5) and (6) to (9), it gives

$$\begin{cases} \dot{\tilde{\boldsymbol{\xi}}}_x = \tilde{\boldsymbol{\xi}}_v \\ \dot{\tilde{\boldsymbol{\xi}}}_v = \boldsymbol{f}(\tilde{\boldsymbol{\xi}}_v) - \alpha(\boldsymbol{L} \otimes \boldsymbol{I}_p)\tilde{\boldsymbol{\xi}} - \beta|(\boldsymbol{L} \otimes \boldsymbol{I}_p)\tilde{\boldsymbol{\xi}}|^{\gamma} \end{cases} \quad (10)$$

Third, determine the following Lyapunov function for the system (3-10):

$$V = V_x + V_v + \tilde{\boldsymbol{\xi}}_x^T \boldsymbol{I}_p \tilde{\boldsymbol{\xi}}_v^T = \tfrac{1}{2}\tilde{\boldsymbol{\xi}}^T \begin{bmatrix} \sigma(\boldsymbol{L} \otimes \boldsymbol{I}_p) & \boldsymbol{I}_p \\ \boldsymbol{I}_p & \boldsymbol{I}_p \end{bmatrix} \tilde{\boldsymbol{\xi}} \quad (11)$$

$$\begin{cases} V_x = \frac{1}{2}\sigma(\boldsymbol{L} \otimes \boldsymbol{I}_p)\tilde{\boldsymbol{\xi}}_x^T \tilde{\boldsymbol{\xi}}_x \\ V_v = \frac{1}{2}\boldsymbol{I}_p \tilde{\boldsymbol{\xi}}_v^T \tilde{\boldsymbol{\xi}}_v \\ \tilde{\boldsymbol{\xi}} = [\tilde{\boldsymbol{\xi}}_x^T \quad \tilde{\boldsymbol{\xi}}_v^T]^T \in \mathbb{R}^{2p} \end{cases} \quad (12)$$

As a result, the following condition must be true for $\sigma \in \mathbb{R}^+$

$$V \geq \tfrac{1}{2}\tilde{\boldsymbol{\xi}}^T \begin{bmatrix} \sigma\lambda_2(\boldsymbol{L}) & 1 \\ 1 & 1 \end{bmatrix} \otimes \boldsymbol{I}_{n\times p} \tilde{\boldsymbol{\xi}} \quad (13)$$

Substituting the following form for (13):

$$V \geq \tfrac{1}{2}\xi^T \begin{bmatrix} \boldsymbol{A} & \boldsymbol{B} \\ \boldsymbol{B}^T & \boldsymbol{C} \end{bmatrix} \otimes \boldsymbol{I}_{n\times p}\xi \tag{14}$$

Furthermore, V is positive using Schur 's complement, if σ is chosen such that $\sigma > \frac{1}{\lambda_2}(\boldsymbol{L})$:

$$\boldsymbol{A} - \boldsymbol{B}\boldsymbol{C}^{-1}\boldsymbol{B}^T = \sigma\lambda_2(\boldsymbol{L}) - 1 > 0 \tag{15}$$

Forth, utilize trajectories (10) to get the time derivative of the function V:

$$\dot{V} = \xi^T \begin{bmatrix} \sigma(\boldsymbol{L}\otimes \boldsymbol{I}_p) & \boldsymbol{I}_p \\ \boldsymbol{I}_p & \boldsymbol{I}_p \end{bmatrix} \dot{\xi}$$

$$= \sigma\xi_x^T(\boldsymbol{L}\otimes \boldsymbol{I}_p)\xi_v + \xi_v^T\boldsymbol{I}_p\xi_v + \xi_x^T\boldsymbol{I}_p\dot{\xi}_v + \xi_v^T\boldsymbol{I}_p\dot{\xi}_v$$

$$= \sigma\xi_x^T(\boldsymbol{L}\otimes \boldsymbol{I}_p)\xi_v + \xi_v^T\boldsymbol{I}_p\xi_v + (\xi_x^T + \xi_v^T)\dot{\xi}_v \tag{16}$$

This is the consequence of applying system dynamics (3-10) to the situation.

$$\dot{V} = \sigma\xi_x^T(\boldsymbol{L}\otimes \boldsymbol{I}_p)\xi_v + \xi_v^T\boldsymbol{I}_p\xi_v + (\xi_x^T + \xi_v^T)\boldsymbol{f}$$
$$-\alpha(\xi_x^T + \xi_v^T)(\boldsymbol{L}\otimes \boldsymbol{I}_p)\xi_x + c(\boldsymbol{L}\otimes \boldsymbol{I}_p)\xi_v$$
$$-\beta(\xi_x^T + \xi_v^T)\left|(\boldsymbol{L}\otimes \boldsymbol{I}_p)\xi_x + c(\boldsymbol{L}\otimes \boldsymbol{I}_p)\xi_v\right|^{\gamma} \tag{17}$$

By adopting Newton's generalized binomial theorem to the setting of the fixed-time graph topology, we demonstrate that

$$\dot{V} = \sigma\xi_x^T(\boldsymbol{L}\otimes \boldsymbol{I}_p)\xi_v + \xi_v^T\boldsymbol{I}_p\xi_v + (\xi_x^T + \xi_v^T)\boldsymbol{f}$$
$$-\alpha(\xi_x^T + \xi_v^T)(\boldsymbol{L}\otimes \boldsymbol{I}_p)\xi_x + c(\boldsymbol{L}\otimes \boldsymbol{I}_p)\xi_v$$
$$-\beta(\xi_x^T + \xi_v^T)\sum_{k=0}^{p}\left\{\binom{\gamma}{k}\left[(\boldsymbol{L}\otimes \boldsymbol{I}_p)\xi_x\right]^{\gamma-k}\left[c(\boldsymbol{L}\otimes \boldsymbol{I}_p)\xi_v\right]^{-k}\right\} \tag{18}$$

Therefore, if we want to show that $\dot{V} < 0$ holds when $\forall t > t_0$, As a starting point, let's consider about the term:

$$\sigma\xi_x^T(\boldsymbol{L}\otimes \boldsymbol{I}_p)\xi_v - \beta(\xi_x^T + \xi_v^T)\sum_{k=0}^{p}\left\{\binom{\gamma}{k}\left[(\boldsymbol{L}\otimes \boldsymbol{I}_p)\xi_x\right]^{\gamma-k}\left[c(\boldsymbol{L}\otimes \boldsymbol{I}_p)\xi_v\right]^{-k}\right\}$$

We put a limit on this term by rewriting it as follows:

$$\sigma\xi_x^T(\boldsymbol{L}\otimes \boldsymbol{I}_p)\xi_v - \beta(\xi_x^T + \xi_v^T)\sum_{k=0}^{p}\left\{\binom{\gamma}{k}\left[(\boldsymbol{L}\otimes \boldsymbol{I}_p)\xi_x\right]^{\gamma-k}\left[c(\boldsymbol{L}\otimes \boldsymbol{I}_p)\xi_v\right]^{-k}\right\} =$$

$$\sigma\xi_x^T(\boldsymbol{L}\otimes \boldsymbol{I}_p)\xi_v - \beta\binom{\gamma}{0}(\xi_x^{\gamma})^T(\boldsymbol{L}\otimes \boldsymbol{I}_p)^{\gamma}\xi_v - \beta\sum_{k=1}^{p}\left\{c^k\binom{\gamma}{k}(\xi_x^{\gamma-k})(\boldsymbol{L}\otimes \boldsymbol{I}_p)^{\gamma}\xi_v^k\right\} =$$

$$\xi_x^T(\boldsymbol{L}\otimes \boldsymbol{I}_p)\xi_v\left[\sigma - \beta\binom{\gamma}{0}(\xi_x^{\gamma-1})^T(\boldsymbol{L}\otimes \boldsymbol{I}_p)^{\gamma-1}\right] - \beta\sum_{k=1}^{p}\left\{c^k\binom{\gamma}{k}(\xi_x^{\gamma-k})(\boldsymbol{L}\otimes \boldsymbol{I}_p)^{\gamma}\xi_v^k\right\} \tag{19}$$

According to the characteristics of the matrix $\boldsymbol{L}$, (19) is limited as follows:

$$\sigma\xi_x^T(\boldsymbol{L}\otimes \boldsymbol{I}_p)\xi_v - \beta(\xi_x^T + \xi_v^T)\sum_{k=0}^{p}\left\{\binom{\gamma}{k}\left[(\boldsymbol{L}\otimes \boldsymbol{I}_p)\xi_x\right]^{\gamma-k}\left[c(\boldsymbol{L}\otimes \boldsymbol{I}_p)\xi_v\right]^{-k}\right\} \leq$$

$$\xi_x^T(\boldsymbol{L}\otimes \boldsymbol{I}_p)\xi_v\left[\sigma - \beta\binom{\gamma}{0}\lambda_2^{\gamma-1}(\boldsymbol{L})\left\|\xi_x^{\gamma-1}\right\|_2\right] - \beta\sum_{k=1}^{p}\left\{c^k\binom{\gamma}{k}(\xi_x^{\gamma-k})(\boldsymbol{L}\otimes \boldsymbol{I}_p)^{\gamma}\xi_v^k\right\} \tag{20}$$

We get that since V_x , is a quadratic function of $\|\xi_x\|$

$$\xi_x^T(\boldsymbol{L}\otimes \boldsymbol{I}_p)\xi_v\left[\sigma - \beta\binom{\gamma}{0}\lambda_2^{\gamma-1}(\boldsymbol{L})\left\|\xi_x^{\gamma-1}\right\|_2\right] - \beta\sum_{k=1}^{p}\left\{c^k\binom{\gamma}{k}(\xi_x^{\gamma-k})(\boldsymbol{L}\otimes \boldsymbol{I}_p)^{\gamma}\xi_v^k\right\} \leq$$

$$\xi_x^T(\boldsymbol{L}\otimes \boldsymbol{I}_p)\xi_v\left[\sigma - \beta\binom{\gamma}{0}\lambda_2^{\gamma-1}(\boldsymbol{L})\left(\frac{2V_x(0)}{\lambda_{max}(\boldsymbol{L})}\right)^{\gamma-1}\right] - \beta\sum_{k=1}^{p}\left\{c^k\binom{\gamma}{k}(\xi_x^{\gamma-k})(\boldsymbol{L}\otimes \boldsymbol{I}_p)^{\gamma}\xi_v^k\right\} \tag{21}$$

By selecting on σ, you will be taken to a

$$\sigma = \beta\binom{\gamma}{0}\lambda_2^{\gamma}(\boldsymbol{L})\left(\tfrac{2V_x(0)}{\lambda_{max}(\boldsymbol{L})}\right)^{\gamma-1} > \tfrac{1}{\lambda_2(\boldsymbol{L})} \tag{22}$$

The gain of control β can be adjusted as

$$\beta > \binom{\gamma}{0}^{-1}\frac{1}{\lambda_2^{\gamma+1}(\boldsymbol{L})}\left(\tfrac{2V_x(0)}{\lambda_{max}(\boldsymbol{L})}\right)^{1-\gamma} \tag{23}$$

When applying (23) to (21), we get

$$\sigma\xi_x^T(\boldsymbol{L}\otimes \boldsymbol{I}_p)\xi_v - \beta\sum_{k=0}^{p}\left\{\binom{\gamma}{k}\left[(\boldsymbol{L}\otimes \boldsymbol{I}_p)\xi_x\right]^{\gamma-k}\left[c(\boldsymbol{L}\otimes \boldsymbol{I}_p)\xi_v\right]^{-k}\right\} \leq$$
$$-\beta\sum_{k=1}^{p}\left\{c^k\binom{\gamma}{k}(\xi_x^{\gamma-k})(\boldsymbol{L}\otimes \boldsymbol{I}_p)^{\gamma}\xi_v^k\right\} \tag{24}$$

Lemma 2: [27] For a vector $\boldsymbol{v} \in \mathbb{R}^n$ with $1_n^T\boldsymbol{v} = 0$ with $1_n = [1,\cdots,1]_n^T$, inequalities involving the following hold $\lambda_{min}(\boldsymbol{M}) > 0$.

$$\begin{cases} \boldsymbol{v}^T\boldsymbol{M}\boldsymbol{v} \geq \lambda_{min}(\boldsymbol{M})\boldsymbol{v}^T\boldsymbol{v} \\ (\boldsymbol{S}\otimes \boldsymbol{I}_N)\boldsymbol{v} \leq \lambda_{max}(\boldsymbol{S})\|\boldsymbol{v}\|_2 \end{cases} \tag{25}$$

It follows from (23) and (24) that

$$\dot{V} \leq \xi_v^T\boldsymbol{I}_p\xi_v - \alpha\lambda_{max}(\boldsymbol{L}\otimes \boldsymbol{I}_p)(\|\xi_x^T\|_2\|\xi_x\|_2 + \|\xi_v^T\|_2\|\xi_x\|_2) + c\,\lambda_{max}(\boldsymbol{L})\|\xi_v\|_2$$
$$-\beta\sum_{k=1}^{p}\left\{c^k\binom{\gamma}{k}(\xi_x^{\gamma-k})(\boldsymbol{L}\otimes \boldsymbol{I}_p)^{\gamma}\xi_v^k\right\} \tag{26}$$

Next, we rewrite (3-17) so that the term $\xi_v^T\boldsymbol{I}_p\xi_v - \alpha(\xi_x^T + \xi_v^T)(\boldsymbol{L}\otimes \boldsymbol{I}_p)\xi_x + c(\boldsymbol{L}\otimes \boldsymbol{I}_p)\xi_v$

$$\dot{V} \leq \xi_v^T\boldsymbol{I}_p\xi_v - \alpha\lambda_{max}(\boldsymbol{L}\otimes \boldsymbol{I}_p)(\|\xi_x^T\|_2\|\xi_x\|_2 + \|\xi_v^T\|_2\|\xi_x\|_2) + c\,\lambda_{max}(\boldsymbol{L})\|\xi_v\|_2$$
$$-\beta\sum_{k=1}^{p}\left\{c^k\binom{\gamma}{k}(\xi_x^{\gamma-k})(\boldsymbol{L}\otimes \boldsymbol{I}_p)^{\gamma}\xi_v^k\right\} \tag{27}$$

Condition $\dot{V} < 0$ holds when $\forall t > t_0$, (27) is found by rearranging as follows:

$$\dot{V} \leq \boldsymbol{\xi}^{T}\boldsymbol{\Upsilon}\boldsymbol{\xi} - \beta\sum_{k=1}^{p}\left\{c^{k}\binom{\gamma}{k}\left(\boldsymbol{\xi}_{x}^{\gamma-k}\right)\left(\boldsymbol{L}\otimes\boldsymbol{I}_{p}\right)^{\gamma}\boldsymbol{\xi}_{v}^{k}\right\} \quad (28)$$

where

$$\begin{cases} \Upsilon_{11} = \beta\delta_{f_i} + 1 \\ \Upsilon_{12} = \Upsilon_{21} = \frac{1}{2}\alpha(1+c)\lambda_{max}\left(\boldsymbol{L}\otimes\boldsymbol{I}_{p}\right) \\ \Upsilon_{22} = \frac{1}{2}\alpha(1+c)\lambda_{max}\left(\boldsymbol{L}\otimes\boldsymbol{I}_{p}\right) \end{cases} \quad (29)$$

It follows from (28) that $\dot{V}$ is negatively definite if and only if

$$\alpha(1+c)\lambda_{max}\left(\boldsymbol{L}\otimes\boldsymbol{I}_{p}\right) - \beta\delta_{f_i} < 0 \quad (30)$$

Which results in

$$\alpha < \frac{\beta\delta_{f_i}}{(1+c)\lambda_{max}(\boldsymbol{L}\otimes\boldsymbol{I}_{p})} \quad (31)$$

IV. Distributed Cooperative Control for UAV MAS

A. UAV MAS Dynamics

Consider a network of n UAVs are operating autonomously, and that the three-dimensional trajectory of each vehicle $i \in N$ is defined by a vector $\boldsymbol{q}_i$ where

$$\boldsymbol{q}_i[\boldsymbol{x}_i, \boldsymbol{\vartheta}_i]^T = [\langle x_i, y_i, z_i\rangle^T, \langle\gamma_i, \theta_i, \psi_i\rangle^T]^T \in \boldsymbol{R^6} \quad (32)$$

Where the position vector is denoted by $\boldsymbol{x}_i$, whereas the angular rotation vector is denoted by $\boldsymbol{\vartheta}_i$, which includes roll, pitch, and yaw. Within the boundaries of the body airframe, the angular velocity vector $\boldsymbol{\omega}_i$ is defined as

$$\boldsymbol{\omega}_i = \begin{bmatrix} 1 & 0 & -sin\theta \\ 0 & cos\gamma & con\theta sin\gamma \\ 0 & sin\gamma & con\theta cos\gamma \end{bmatrix}\dot{\boldsymbol{\vartheta}}_i \quad (33)$$

All of the following agent and leader dynamic models are considered as following

Agents:

$$\begin{cases} \dot{\boldsymbol{x}}_i = \boldsymbol{v}_i, \dot{\boldsymbol{v}}_i = \boldsymbol{f}_{it} + \boldsymbol{u}_{it} \\ \dot{\vartheta}_i = \omega_i, \dot{\omega}_i = \boldsymbol{f}_{ir} + \boldsymbol{u}_{ir} \end{cases} \quad (34)$$

Leader:

$$\begin{cases} \dot{\boldsymbol{x}}_0 = \boldsymbol{v}_0, \dot{\boldsymbol{v}}_0 = \boldsymbol{f}_{t0} \\ \dot{\vartheta}_0 = \boldsymbol{T}^{-1}\omega_0, \dot{\omega}_0 = \boldsymbol{f}_{r0} \end{cases} \quad (35)$$

where t and r denote translational and rotational motions, respectively; $f_{it} = T^{-1}f_{t0}$, $f_{it} = f_{r0}$; T is the matrix that connects the body frame to the inertial frame; it is obtained, from Euler rotations, as

$$\boldsymbol{T} = \begin{bmatrix} T_{11} & T_{12} & T_{13} \\ T_{21} & T_{22} & T_{23} \\ T_{31} & T_{32} & T_{33} \end{bmatrix} \quad (36)$$

where

$$\begin{cases} T_{11} = cos\gamma cos\psi - cos\theta sin\gamma sin\psi \\ T_{12} = -cos\psi sin\gamma - cos\gamma cos\theta sin\psi \\ T_{13} = sin\theta sin\psi \\ T_{21} = cos\theta cos\psi sin\gamma - cos\gamma sin\psi \\ T_{22} = cos\gamma cos\theta cos\psi - sin\gamma sin\psi \\ T_{23} = -cos\psi sin\theta \\ T_{31} = sin\gamma sin\theta \\ T_{32} = cos\gamma sin\theta \\ T_{33} = cos\theta \end{cases}$$

B. UAV MAS Consensus Control

Lemma 3: Theorem 1 is used to construct the $\boldsymbol{u}_{it}$ and $\boldsymbol{u}_{ir}$ control inputs for translation and rotation, respectively.

$$\begin{cases} \boldsymbol{u}_{it}(t) = -\alpha_t\,\boldsymbol{e}_{it} - \beta_t\,|\boldsymbol{e}_{it}|^{\gamma} \\ \boldsymbol{u}_{ir}(t) = -\alpha_r\,\boldsymbol{e}_{ir} - \beta_r\,|\boldsymbol{e}_{ir}|^{\gamma} \end{cases} \quad (37)$$

where α_t, β_t, α_r, and β_r are computed by using (23) and (30), and

$$\begin{cases} \mathrm{A}_{it}(t) = \sum_{j=0}^{n} a_{ij}\left(\boldsymbol{x}_i(t) - \boldsymbol{x}_j(t)\right) \\ \quad +c\sum_{j=0}^{n} a_{ij}\left(\boldsymbol{v}_i(t) - \boldsymbol{v}_j(t)\right) \\ \mathrm{A}_{ir}(t) = \sum_{j=0}^{n} a_{ij}\left(\boldsymbol{\vartheta}_i(t) - \boldsymbol{\vartheta}_j(t)\right) \\ \quad +c\sum_{j=0}^{n} a_{ij}\left(\boldsymbol{\omega}_i(t) - \boldsymbol{\omega}_j(t)\right) \end{cases} \quad (38)$$

C. UAV MAS Formation Control

The goal of formation control is to develop translational and rotational controls that allow multi-UAVs to precisely track a predetermined geometric pattern $\mathcal{P}(x, y, z)$ in three-dimensional space with

$$\sum_{i=1}^{n} p_{ix} = p_{0x}, \sum_{i=1}^{n} p_{iy} = p_{0y}, \sum_{i=1}^{n} p_{iz} = p_{0z} \quad (39)$$

Where (p_{0x}, p_{0y}, p_{0z}) is the center of the geometric pattern $\mathcal{P}(x, y, z)$.

In this scenario, we assume that the formation states are denoted by that η_{1i}, η_{2i} and, η_{3i}, and that the formation control protocols are denoted by u_{1i} and, u_{2i}, and that the formation evolves according to the following dynamics system [28]:

$$\begin{cases} \dot{\eta}_{1i} = u_{1i} \\ \dot{\eta}_{2i} = u_{2i} \\ \dot{\eta}_{3i} = u_{1i}\eta_{2i} - k_0|u_{1i}|\eta_{3i} \end{cases} \quad (40)$$

where $k_0 \in \mathbb{R}^{+}$. The following illustrates how the trajectories of the agents relate to the pattern's trajectory:

$$\begin{cases} x_i = \cos(\eta_{1i})\left[\eta_{2i} - k_0\mathrm{sign}(u_{1i})\eta_{3i}\right] + \sin(\eta_{1i})\,\eta_{3i} + p_{xi} \\ y_i = \sin(\eta_{1i})\left[\eta_{2i} - k_0\mathrm{sign}(u_{1i})\eta_{3i}\right] + \cos(\eta_{1i})\,\eta_{3i} + p_{yi} \\ z_i = p_{zi} \end{cases} \quad (41)$$

If $\lim_{t\to\infty}(\eta_{ki} - \eta_{k0}) = 0$ and $\lim_{t\to\infty}(u_{li} - u_{l0}) = 0$ for $k = 1,2,3; l = 1,2; 1 \leq i \leq n$, then for $1 \leq i \neq j \leq n$ the MAS of n-UAV achieves

$$\lim_{t\to\infty}\begin{bmatrix} \mathrm{x_i} - \mathrm{x_j} \\ \mathrm{y_i} - \mathrm{y_j} \\ \mathrm{z_i} - \mathrm{z_j} \end{bmatrix} = \begin{bmatrix} \mathrm{p_{xi}} - \mathrm{p_{xj}} \\ \mathrm{p_{yi}} - \mathrm{p_{yj}} \\ \mathrm{p_{zi}} - \mathrm{p_{zj}} \end{bmatrix}, \lim_{t\to\infty}\left(\sum\frac{\mathrm{x_i}}{\mathrm{n}} - \mathrm{x_0}\right)_{\mathrm{i=1}}^{\mathrm{n}} = 0,$$
$$\lim_{t\to\infty}\left(\sum_{i=1}^{n}\frac{y_i}{n} - y_0\right) = 0, \lim_{t\to\infty}\left(\sum_{i=1}^{n}\frac{z_i}{n} - z_0\right) = 0 \quad (42)$$

where the leader coordinates are denoted by x_0, y_0, z_0 respectively (the formation pattern centroid). The definition of the vector $\tilde{\eta}_i = [(\eta_{1i} - \eta_{10}), (\eta_{2i} - \eta_{20}), (\eta_{3i} - \eta_{30})]^{\mathrm{T}}$ as the tracking error vector for each UAV$_i$ and applying control law (5) to both u_{1i} and u_{2i}, we are able to establish that

$$\begin{cases} u_{ki} = -\alpha_k \mathrm{A}_{ki} - \beta_k |\mathrm{A}_{ki}|^{\gamma} \\ \mathrm{A}_{ki}(t) = \sum_{j=0}^{n} a_{ij} \left(\eta_{ki}(t) - \eta_{kj}(t)\right) \end{cases}, k = 1,2. \quad (43)$$

Following is the reduced dynamic system that is generated as a result of substituting protocols (42) into the first two dynamic equations of the system (39):

$$\begin{cases} \dot{\tilde{\eta}}_{1i} = -\alpha_1 \sum_{j=0}^{n} a_{ij} \left(\eta_{1i}(t) - \eta_{1j}(t)\right) \\ -\beta_1 \left|\sum_{j=0}^{n} a_{ij} \left(\eta_{1i}(t) - \eta_{1j}(t)\right)\right|_i^{\gamma} + \dot{\eta}_{10} \\ \dot{\tilde{\eta}}_{2i} = -\alpha_2 \sum_{j=0}^{n} a_{ij} \left(\eta_{2i}(t) - \eta_{2j}(t)\right) \\ -\beta_2 \left|\sum_{j=0}^{n} a_{ij} \left(\eta_{2i}(t) - \eta_2(t)\right)\right|_i^{\gamma} + \dot{\eta}_{20} \end{cases} \quad (44)$$

In the form of a vector, equation (44) is identical to the auxiliary closed-loop system that is presented in the following:

$$\dot{\tilde{\eta}} = -\alpha(\boldsymbol{L} \otimes \boldsymbol{I}_2)\tilde{\eta} - \beta|(\boldsymbol{L} \otimes \boldsymbol{I}_2)\tilde{\eta}|^{\gamma} - \dot{\eta}_0 \quad (45)$$

where

$$\tilde{\eta} = [\tilde{\eta}_1^T, \ \tilde{\eta}_2^T]^T = [\tilde{\eta}_{11}, \cdots, \tilde{\eta}_{1n}, \ \tilde{\eta}_{21}, \cdots, \tilde{\eta}_{2n}]^T$$
$$\tilde{\boldsymbol{\eta}}_0 = [\mathbf{1}_n^T \tilde{\eta}_{10}, \ \mathbf{1}_n^T \tilde{\eta}_{20}]^T$$
$$\boldsymbol{\alpha} = \begin{bmatrix} \alpha_1 \boldsymbol{I}_n & \mathbf{0}_{nn} \\ \mathbf{0}_{nn} & \alpha_2 \boldsymbol{I}_n \end{bmatrix}, \boldsymbol{\beta} = \begin{bmatrix} \beta_1 \boldsymbol{I}_n & \mathbf{0}_{nn} \\ \mathbf{0}_{nn} & \beta_2 \boldsymbol{I}_n \end{bmatrix}$$

Theorem 2: Considering Assumptions 1-3 hold true, the communication graph $\boldsymbol{\mathcal{G}}$ is connected and the control inputs to the closed-loop system (46) are selected according to (43), the agents' states η_{1i} and η_{2i} will converge to the formation states η_{10} and η_{20}, respectively, if the tracking error converges to zero $\lim_{t\to\infty}(\tilde{\eta}_i) = 0$.

Proof: The following quadratic function can be considered of as a potential Lyapunov function

$$V = \frac{1}{2}\tilde{\eta}^{\mathrm{T}}(\boldsymbol{L} \otimes \boldsymbol{I}_2)\tilde{\eta} \quad (46)$$

If we assume that V is continuously differentiable with regard to ζ, we may formulate its time derivative $\dot{V}$ as

$$\dot{V} = \tilde{\eta}^{\mathrm{T}}(\boldsymbol{L} \otimes \boldsymbol{I}_2)\dot{\tilde{\eta}} \quad (47)$$

If the auxiliary closed-loop system (45) is used, we obtain

$$\dot{V} = -\alpha\tilde{\eta}^{\mathrm{T}}(\boldsymbol{L} \otimes \boldsymbol{I}_2)\tilde{\eta} - \beta\tilde{\eta}^{\mathrm{T}}(\boldsymbol{L} \otimes \boldsymbol{I}_2)|(\boldsymbol{L} \otimes \boldsymbol{I}_2)\tilde{\eta}|^{\gamma} - \dot{\eta}_0 \quad (48)$$

Since $\gamma > 0$ and the gain matrices $\boldsymbol{\alpha}$ and $\boldsymbol{\beta}$ are both diagonal, we have

$$\dot{V} \leqslant -det(\boldsymbol{\alpha})\tilde{\eta}^T(\boldsymbol{L} \otimes \boldsymbol{I}_2)\,\tilde{\eta}$$
$$-\det(\boldsymbol{\beta})\,\eta^{\mathrm{T}}(\boldsymbol{L} \otimes \boldsymbol{I}_2)|(\boldsymbol{L} \otimes \boldsymbol{I}_2)\tilde{\eta}|^{\gamma} \quad (49)$$

Furthermore, the inequation (49) satisfies

$$\dot{V} \leqslant -\det(\boldsymbol{\alpha})\,\lambda_{\min}^2(\boldsymbol{L} \otimes \boldsymbol{I}_2)\parallel \tilde{\eta} \parallel_2^2 \quad (50)$$

Since $V = \frac{1}{2}\tilde{\eta}^{\mathrm{T}}(\boldsymbol{L} \otimes \boldsymbol{I}_2)\tilde{\eta} \leqslant \frac{1}{2}\lambda_{\max}(\boldsymbol{L} \otimes \boldsymbol{I}_2) \parallel \tilde{\eta} \parallel_2^2$ and $\lambda_i(\boldsymbol{L} \otimes \boldsymbol{I}_2) = \lambda_i(\boldsymbol{L})$, it follows that

$$\dot{V} \leqslant -\det(\boldsymbol{\alpha})\frac{\sqrt{2}\lambda_{\min}^2(\boldsymbol{L})}{\sqrt{\lambda_{\max}(\boldsymbol{L})}}\sqrt{V} \quad (51)$$

It is concluded from (51) that

$$\sqrt{V} \leqslant \sqrt{V_0} - \frac{\det(\boldsymbol{\alpha})}{\sqrt{2}}\frac{\lambda_{\min}^2(\boldsymbol{L})}{\sqrt{\lambda_{\max}(\boldsymbol{L})}}t \quad (52)$$

Formation tracking is guaranteed to converge if and only if $\sqrt{V} = 0$

$$t \geqslant \sqrt{V_0}\frac{\sqrt{2}}{\det(\boldsymbol{\alpha})}\frac{\sqrt{\lambda_{\max}(\boldsymbol{L})}}{\lambda_{\min}^2(\boldsymbol{L})}$$
$$= \frac{\sqrt{\tilde{\zeta}^{\mathrm{T}}(0)(\boldsymbol{L}\otimes\boldsymbol{I}_2)\tilde{\zeta}(0)}}{\det(\boldsymbol{\alpha})}\frac{\sqrt{\lambda_{\max}(\boldsymbol{L})}}{\lambda_{\min}^2(\boldsymbol{L})} \quad (53)$$

V. SIMULATION

A. Consensus of Formation Pattern

Here, a team of n = 4 UAVs performs out a path-following mission within a simulated environment. As illustrated in Fig. 1, the path under consideration follows a half-parabolic shape. A swarm of UAVs forms in a specified formation is shown in Fig. 2 (a), following the common trajectory. Using the topology depicted in Fig. 2 (b), they track together a predetermined 3D trajectory through space.

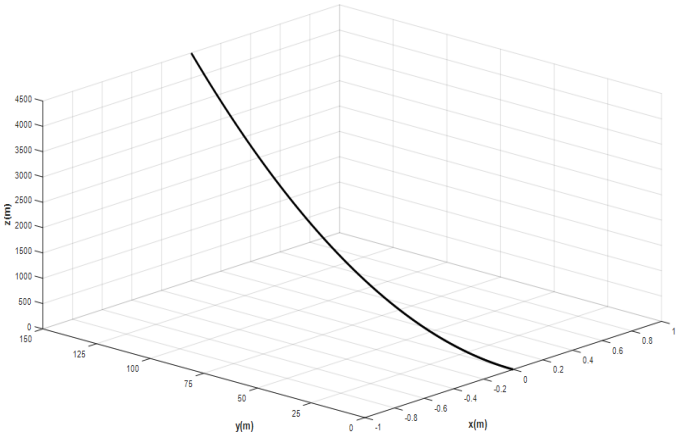

Fig. 1. Desired formation and trajectory.

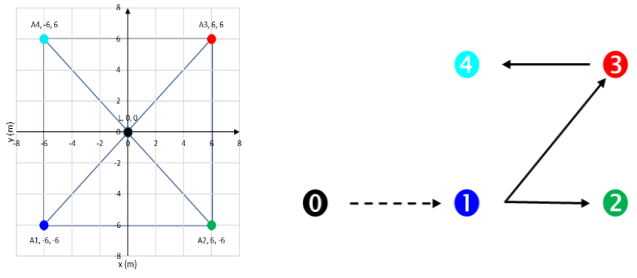

(a) Desired formation (b) Communication topology graph

Fig. 2. Desired formation and fixed-time directed communication topology graph.

Fig. 3 illustrates the consensus in three dimensions among the four agents, as well as the timeline of how the agents' orientations gradually approach those of the virtual leader. Meanwhile, Fig. 4 illustrates the path taken for the leader and the followers by the centroid formation as it moves along the motion axes.

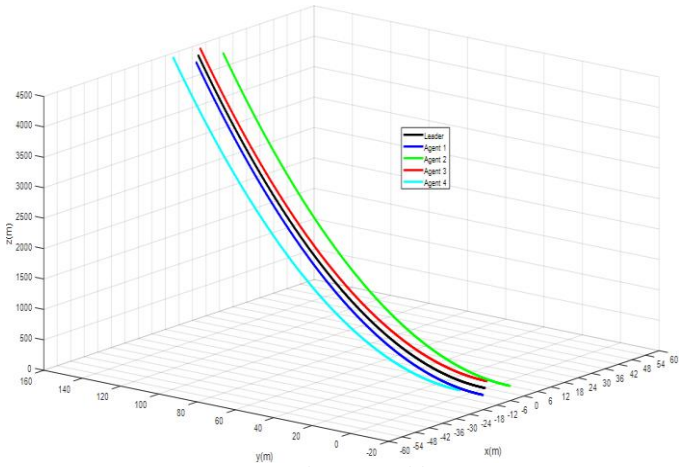

(a) Consensus of the team of four agents.

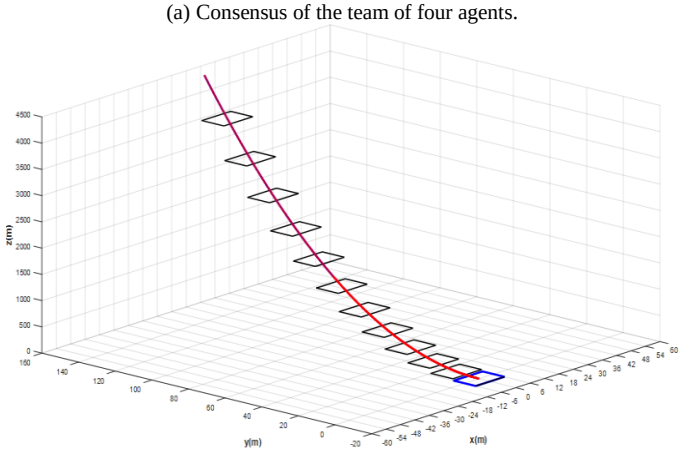

(b) Agents' orientations.

Fig. 3. Formation tracking with the control law.

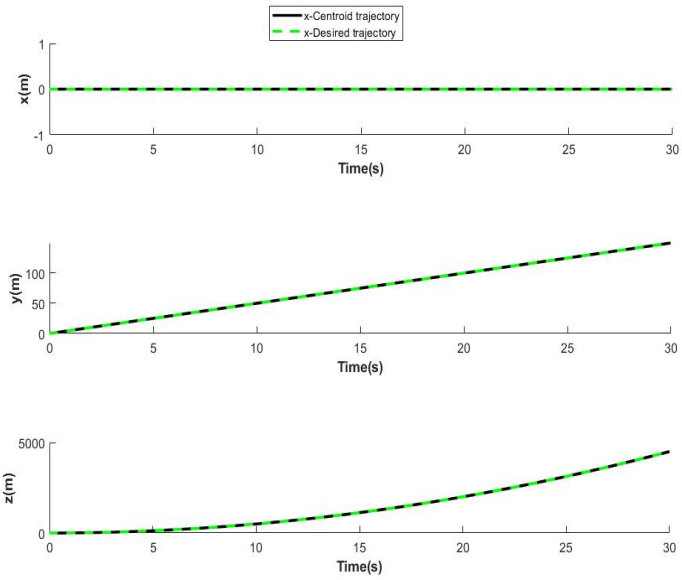

Fig. 4. Geometric pattern centroid tracking.

B. *Tracking of Formation Pattern*

Within the context of the simulated scenario, a team of four UAVs performs out a routing path following mission. Parametric trajectories take into account the considered path as defined by:

$$\begin{cases} x = \frac{x_0 + \cos^{-1} t - b\, r \sin t}{\sqrt{a^2+b^2}} \\ y = \frac{y_0 + \cos^{-1} t - b\, r \sin t}{\sqrt{a^2+b^2}} \\ z = z_0 + r \cos t\ \sqrt{a^2+b^2} \end{cases} \quad (54)$$

With $a = 10$, $b = 10$, and $r = 50$

The formation mission can be accomplished with a switching communication topology like that illustrated in Fig. 5 and a dwell duration of 15 s.

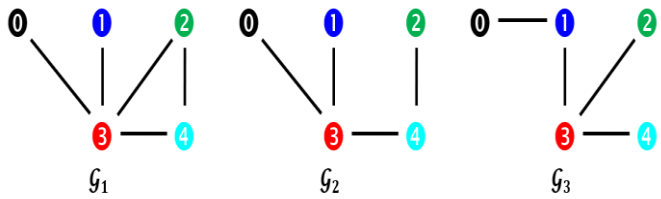

Fig. 5. Switching undirected topology interaction graph.

Fig. 6 illustrates how the proposed control law was applied to the formation tracking.

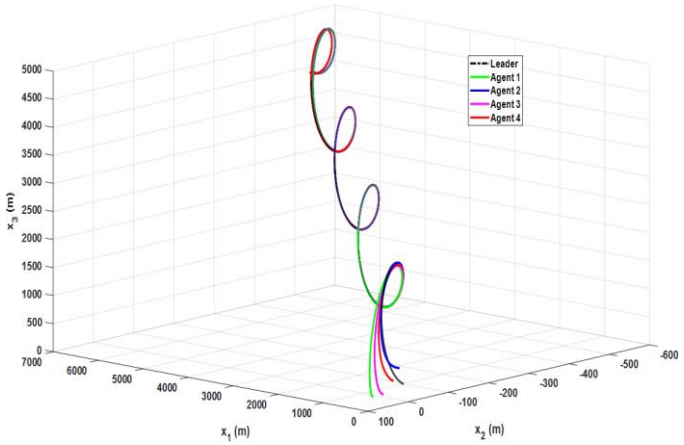

Fig. 6. Formation tracking with the proposed control law.

Fig. 3 to 6 show that the four UAVs achieved the formation requirements with the proposed distributed protocol despite the complex communication limitations and dynamic constraints. the tracking error of the formation is 0, as shown in Fig. 3. This demonstrates that the distributed formation control protocol is successful for UAV formation even under communication loss and topology switching conditions. If the formation of the UAVs needs to be adjusted while they are in flight, the control protocol can be used even when the UAVs' configuration changes dynamically. The results of the simulation demonstrate the effectiveness of the proposed control scheme.

VI. Conclusion

Based on leader-following consensus in MAS, a smooth distributed cooperative control for multi-air vehicles such as UAVs was designed. First, we developed smooth distributed consensus protocols, as opposed to the traditional sliding-mode based algorithms, by substituting the discontinuous signum function with a continuous integral function. Then, a model for flying formation control was developed to track and maintain three-dimensional geometric patterns. A Lyapunov function-based approach was used to set the necessary and sufficient requirements for the convergence of both consensus and formation algorithms. The primary focus of the presented study in the near future will be on event-based formation control for multi-UAV systems, formation tracking in harsh environments, obstacle avoidance and disturbance rejections among aerial moving agents.

Acknowledgment

This project was funded by the Deanship of Scientific Research (DSR), King Abdulaziz University, Jeddah, under grant No. (KEP-2-135-42). The authors, therefore, gratefully acknowledge DSR technical and financial support.

References

[1] B. Kada, A. S. A. Balamesh, K. A. Juhany, and I. M. Al-Qadi, "Distributed cooperative control for nonholonomic wheeled mobile robot systems," Int J Syst Sci, vol. 51, no. 9, pp. 1528–1541, Jul. 2020, doi: 10.1080/00207721.2020.1765048.

[2] A. Y. Tameem, B. Kada, and A. A. Alzubairi, "Formation Control with Switching Topology for Multi-agent Nonholonomic Wheeled Mobile Robot Systems," 2022 IEEE IAS Global Conference on Emerging Technologies, GlobConET 2022, pp. 276–281, 2022, doi: 10.1109/GLOBCONET53749.2022.9872448.

[3] Y. Liu and A. Zhang, "Cooperative task assignment method of manned/unmanned aerial vehicle formation," Systems engineering and electronics, vol. 32, no. 3, pp. 584–588, 2010.

[4] W. Lin, "Distributed UAV formation control using differential game approach," Aerosp Sci Technol, vol. 35, pp. 54–62, 2014.

[5] H. Du, W. Zhu, G. Wen, Z. Duan, and J. Lü, "Distributed formation control of multiple quadrotor aircraft based on nonsmooth consensus algorithms," IEEE Trans Cybern, vol. 49, no. 1, pp. 342–353, 2017.

[6] Z. Liang, L. U. Yi, X. U. Shida, and F. Han, "Multiple UAVs cooperative formation forming control based on back-stepping-like approach," Journal of Systems Engineering and Electronics, vol. 29, no. 4, pp. 816–822, 2018.

[7] B. Zhang, X. Sun, S. Liu, and X. Deng, "Adaptive differential evolution-based distributed model predictive control for multi-UAV formation flight," International Journal of Aeronautical and Space Sciences, vol. 21, no. 2, pp. 538–548, 2020.

[8] X. Dong, Y. Hua, Y. Zhou, Z. Ren, and Y. Zhong, "Theory and Experiment on Formation-Containment Control of Multiple Multirotor Unmanned Aerial Vehicle Systems," IEEE Transactions on Automation Science and Engineering, vol. 16, no. 1, pp. 229–240, Jan. 2019, doi: 10.1109/TASE.2018.2792327.

[9] Z. Ziyang, Z. H. U. Ping, X. U. E. Yixuan, and J. I. Yuxuan, "Distributed intelligent self-organized mission planning of multi-UAV for dynamic targets cooperative search-attack," Chinese Journal of Aeronautics, vol. 32, no. 12, pp. 2706–2716, 2019.

[10] J. W. Hu, M. Wang, C. H. Zhao, Q. Pan, and C. Du, "Formation control and collision avoidance for multi-UAV systems based on Voronoi partition," Science China Technological Sciences 2019 63:1, vol. 63, no. 1, pp. 65–72, Sep. 2019, doi: 10.1007/S11431-018-9449-9.

[11] S. Shao, Y. Peng, C. He, and Y. Du, "Efficient path planning for UAV formation via comprehensively improved particle swarm optimization," ISA Trans, vol. 97, pp. 415–430, Feb. 2020, doi: 10.1016/J.ISATRA.2019.08.018.

[12] B. Kada, M. Khalid, and M. S. Shaikh, "Distributed cooperative control of autonomous multi-Agent UAV systems using smooth control," Journal of Systems Engineering and Electronics, vol. 31, no. 6, pp. 1297–1307, Dec. 2020, doi: 10.23919/JSEE.2020.000100.

[13] J. K. Verma and V. Ranga, "Multi-Robot Coordination Analysis, Taxonomy, Challenges and Future Scope," J Intell Robot Syst, vol. 102, no. 1, pp. 1–36, 2021.

[14] Z. Meng, Z. Lin, and W. Ren, "Robust cooperative tracking for multiple non-identical second-order nonlinear systems," Automatica, vol. 49, no. 8, pp. 2363–2372, 2013.

[15] A. Karimoddini, H. Lin, B. M. Chen, and T. H. Lee, "Hybrid three-dimensional formation control for unmanned helicopters," Automatica, vol. 49, no. 2, pp. 424–433, 2013.

[16] J. Zhang, D. Ye, J. D. Biggs, and Z. Sun, "Finite-time relative orbit-attitude tracking control for multi-spacecraft with collision avoidance and changing network topologies," Advances in Space Research, vol. 63, no. 3, pp. 1161–1175, Feb. 2019, doi: 10.1016/J.ASR.2018.10.037.

[17] Y. Guo, J. Zhou, and Y. Liu, "Distributed RISE control for spacecraft formation reconfiguration with collision avoidance," J Franklin Inst, vol. 356, no. 10, pp. 5332–5352, Jul. 2019, doi: 10.1016/J.JFRANKLIN.2019.05.003.

[18] A. Alzubairi, B. Kada, and A. Tameem, "Decentralized Cooperation Control for Formation Flying Spacecraft," 2022 IEEE IAS Global Conference on Emerging Technologies, GlobConET 2022, pp. 187–190, 2022, doi: 10.1109/GLOBCONET53749.2022.9872513.

[19] A. Alzubairi, B. Kada, and A. Tameem, "Attitude Consensus Control of Spacecraft Formation Flying: Model-Based Design," in 72nd International Astronautical Congress (IAC), Dubai, United Arab Emirates: the International Astronautical Federation (IAF), Oct. 2021.

[20] P. O. Skobelev, E. V. Simonova, A. A. Zhilyaev, and V. S. Travin, "Application of Multi-agent Technology in the Scheduling System of Swarm of Earth Remote Sensing Satellites," Procedia Comput Sci, vol. 103, pp. 396–402, Jan. 2017, doi: 10.1016/J.PROCS.2017.01.127.

[21] Z. Zheng, J. Guo, and E. Gill, “Distributed onboard mission planning for multi-satellite systems,” Aerosp Sci Technol, vol. 89, pp. 111–122, Jun. 2019, doi: 10.1016/J.AST.2019.03.054.

[22] X. Liu, L. Liu, and Y. Wang, “Minimum time state consensus for cooperative attack of multi-missile systems,” Aerosp Sci Technol, vol. 69, pp. 87–96, Oct. 2017, doi: 10.1016/J.AST.2017.06.016.

[23] T. Lyu, Y. Guo, C. Li, G. Ma, and H. Zhang, “Multiple missiles cooperative guidance with simultaneous attack requirement under directed topologies,” Aerosp Sci Technol, vol. 89, pp. 100–110, Jun. 2019, doi: 10.1016/J.AST.2019.03.037.

[24] A. Almalki and B. Kada, “Consensus tracking for multiagent systems under bounded unknown external disturbances using sliding-PID control,” Int J Sci Basic Appl Res, vol. 50, no. 2, pp. 143–153, 2020.

[25] T., Canhui, R. Zhang, Z. Song, B. Wang, and Y. Jin. "Multi-UAV Formation Control in Complex Conditions Based on Improved Consistency Algorithm" Drones, vol. 7, no. 3: 2023. https://doi.org/10.3390/drones7030185

[26] J. Li, J. Liu, S. Huangfu, G. Cao, and D. Yu. “Leader-follower formation of light-weight UAVs with novel active disturbance rejection control,” Applied Mathematical Modelling, vol. 117, pp. 577-591, 2023. https://doi.org/10.1016/j.apm.2022.12.032.

[27] S. Li, H. Du, and X. Lin, “Finite-time consensus algorithm for multi-agent systems with double-integrator dynamics,” Automatica, vol. 47, no. 8, pp. 1706–1712, 2011.

[28] Z. Peng, S. Yang, G. Wen, A. Rahmani, and Y. Yu, “Adaptive distributed formation control for multiple nonholonomic wheeled mobile robots,” Neurocomputing, vol. 173, pp. 1485–1494, 2016.